# Observations of Far-Infrared Fine Structure Lines: [O III] 88.35μm and [O I] 63.2μm*



J.W.V. Storey, D.M. Watson and C.H. Townes
Department of Physics
University of California, Berkeley

Received_____

## ABSTRACT

Observations of the [O III] 88.35μm line and the [O I] 63.2μm line have been made with a new far-infrared spectrometer. The sources M17, NGC 7538 and W51 have been mapped in the [O III] line with 1 arcminute resolution and the emission is found to be quite widespread. In all cases we find that the peak of the emission coincides with the maximum radio continuum. Where possible we have simultaneously mapped the far-infrared continuum and in M17, NGC 7538 and W51 the continuum peak is found to be distinct from the center of ionization. The [O III] line was also detected in W3, W49 and in a number of positions in the Orion nebula. Upper limits were obtained on NGC 7027, NGC 6572, DR21, G29.9-0.0 and M82. The 63.2μm [O I] line has been detected in M17, M42, and marginally in DR21. A partial map of M42 in this line shows that most of the emission observed arises from

*This work is supported in part by NASA Grant NGR 05-003-511.

the Trapezium and from the bright optical bar to the southeast. The J=1→0 transition of HD at 112μm was also searched for in the direction of the Kleinmann-Low nebula, but without success.

# I. INTRODUCTION

Far-infrared fine structure lines provide a particularly useful means of studying ionic species in H II regions, planetary nebulae and galaxies. Development of this field has only become possible in recent years with the provision of high altitude telescopes such as the Kuiper Airborne Observatory. The first detection of [O III] $\lambda$ = 88.35μm was by Ward et al. (1975) in M17. Since then, the same line has been detected in Orion (Baluteau et al. 1976 and Moorwood et al. 1978) and in several other H II regions (Dain et al. 1978). So far the sources have either been observed with large beams, or the signal-to-noise ratio has been too low to produce detailed maps. We present in this paper the first far-infrared fine structure line maps, which were taken at a resolution of 1 arc minute.

In general, the distribution of [O III] emission can be expected to resemble that of the radio continuum (since both arise from electron collisions) but with some important differences. First, the radio continuum (free-free emission) is proportional to the emission measure or electron density squared, while the fine structure line is, except at very low densities, proportional to ionic column density and hence in most cases varies linearly with the electron density. Secondly, the abundance of $O^{++}$ relative to hydrogen is not necessarily constant from cloud to cloud, or indeed within a cloud. Apart from variations in the local oxygen abundance, molecules and grain surfaces can lower the effective atomic

oxygen content of the gas. Furthermore, the intensity and effective temperature of the ionizing radiation will affect the relative abundance of $O^{++}$. Because 35.11 eV is required to ionize oxygen to $O^{++}$, and 55.89 eV to ionize it further, $O^{++}$ is an abundant species in many H II regions but may sometimes appear depleted when the exciting star is cool. Comparison of radio and fine structure maps, particularly where differences exist, thus provides information on the spectral type of the stars underlying the H II region, and may possibly shed some light on their formation. Comparison with fine structure lines of other ions would also yield important information. An interesting example is [S IV] at 10.5μ. Although this ion has a very similar ionization requirement (34.83 eV) to [O III], much higher electron densities are needed to reach thermal equilibrium.

The [O I] line at 63.2μm is of particular interest because it can be excited not only by the ionized material in H II regions, but also by warm, neutral atoms in post-shock gas (Hill and Hollenbach, 1978). The [O I] line has recently been detected in M42 and M17 by Melnick et al. (1979a) but the large beam-size used (4 x 6 arcminutes) leaves unanswered the question of what kind of conditions are producing the emission. We have confirmed the presence of [O I] in M17, and in M42 examined each of the regions most likely to produce the emission.

Detection of HD in molecular clouds would be a very direct way of determining the D/H ratio in these regions.

Several deuterated molecules have already been detected by radio techniques, but uncertainties about the exact nature of the chemical fractionation processes involved in the formation of these molecules make the results extremely difficult to interpret. However, because molecular hydrogen is the principal species in these clouds by such an enormous margin, the $HD/H_2$ ratio is an accurate representation of the cloud D/H ratio. In addition, rotational transitions of HD may be significant in the overall cooling of molecular clouds. A preliminary search has hence been undertaken for this molecule.

## II. INSTRUMENTATION AND OBSERVATIONS

The spectrometer uses a fixed wavelength Fabry-Perot interferometer cooled to 4.2 K in conjunction with a high order scanning Fabry-Perot at room temperature. The scanning Fabry-Perot, although warm, is placed immediately outside the cold aperture stop in such a way that at wavelengths outside its narrow passbands it reflects only liquid helium temperatures into the detector. High resolution is thus obtained while minimizing the thermal background radiation on the detector. Because only a narrow range of wavelengths is incident on the detector at any one time, "guiding" noise and fluctuations in the atmospheric water vapor content along the line of sight do not contribute significantly to the system noise. The Fabry-Perot mirrors consist of gold-plated nickel mesh stretched tightly over invar rings; each filter has a finesse

of about 35. Short-wavelength radiation is blocked by a 2 mm thick $BaF_2$ filter (AR coated) and a quartz/diamond scatter/$CaF_2$ filter, both at 4.2 K. The detector is a 4.2 K gallium-doped germanium photoconductor mounted in an integrating cavity, both kindly lent to us by K. Shivanandan.

The spectrometer resolution was determined in the laboratory by scanning across the output of a far-infrared methanol laser operating at 96.5μm and at 118.8μm. The response profile is a lorentzian (as expected for a Fabry-Perot system) with a full width at half maximum of 0.12μm when the system is used in 20th order.

The observations were made with the 91.4 cm telescope of the Kuiper Airborne Observatory in four flights during September, 1978, at an altitude of 41,000 feet (12.5 km). An oscillating secondary mirror chopped the beam in azimuth by between two and six arcminutes (depending on the source) at a frequency of 35 Hz. A typical observation consists of a 40 second scan with the source in one beam followed by an equal time with the source in the other beam. The detector output is amplified by a room temperature JFET amplifier, then synchronously detected at 35 Hz. After passing through a six-pole low pass Bessel filter the output is sampled 1024 times each scan and the result stored on magnetic tape for later analysis.

Wavelength calibration was performed in flight by observing a gas cell containing $H_2O$, $H_2{}^{18}O$ or HDO, chopped

against a 100°C blackbody. The same blackbody was monitored frequently during observations to check for drifts in sensitivity. Absolute intensities were calibrated by observation of Jupiter and by the expected continuum of the nebulae themselves. The absolute calibration uncertainty is of the order of 30%, although when mapping a given source the relative uncertainty across the map is much less. The measured beamwidth was 1 arcminute (full width at half maximum) but observation of extended sources shows that the effective area of the beam was equivalent to that of a 75 arcsecond disc. Pointing was determined by offset from guide stars and is accurate to within 15 arcseconds.

At 88μm the instrumental resolving power ($\lambda/\delta\lambda$) was 700, with a system NEP in flight of $1.4 \times 10^{-13} W/\sqrt{Hz}$ (including all telescope and spectrometer losses). At 63 and 112μm the performance was not as good, due partly to mistuning of the 63μm filter, and partly because the scanning Fabry-Perot was operated in lower orders, limiting the resolution.

## III. THEORY

### a) [O III] $\lambda$ = 88.35μm

Russell-Saunders coupling is a good approximation for the ground term of $O^{++}$, which is $^{2S+1}L_J = {}^3P_{2,1,0}$. Levels of different J in this term are split by the spin-orbit interaction into a normal triplet (see Figure 1). Since all of these levels have the same parity, there can be no electric dipole transitions between them. The lowest-order transitions are the magnetic dipole (M1) transitions ${}^3P_2 \rightarrow {}^3P_1$ and

$^3P_1 \rightarrow {}^3P_0$, and the electric quadrupole (E2) transitions $^3P_2 \rightarrow {}^3P_0$ and $^3P_2 \rightarrow {}^3P_1$. The M1 transitions, having Einstein A-coefficients of $\sim 10^{-5}\,sec^{-1}$, are the brighter by factors of about $10^6$. These transitions are easily excited and de-excited by the magnetic fields of passing electrons.

Typical electron densities of H II regions are in the range $400\ cm^{-3} \lesssim N_e \lesssim 10^4 cm^{-3}$, with temperatures in the range $5 \times 10^3 K \lesssim T \lesssim 10^4 K$. Under such conditions, the populations of the fine structure levels of the ground term of $O^{++}$ are close to the thermal equilibrium values, which in turn are close to the statistical weights for the states because $kT >> E$. The radiation from the ionized clouds in the $^3P_2 \rightarrow {}^3P_1$ ($\lambda = 51.8\mu m$) and $^3P_1 \rightarrow {}^3P_0$ ($\lambda = 88.35\mu m$) transitions is optically thin. These facts imply a very simple expression for the power per unit area and solid angle in these lines:

$$I_{(k\rightarrow j)} = \frac{hc}{4\pi\lambda} A_{kj} n_k \ell \qquad (1)$$

where $A_{kj}$ is the A-coefficient for the transition, $n_k$ the density of $O^{++}$ ions in the upper state k, and $\ell$ is the length of the nebula along the line of sight. $n_k$ can be related to the total density n of $O^{++}$ ions by

$$n_k = \frac{f_k n}{1+f_1+f_2}$$

where k = 1,2, and $f_1 \equiv \frac{n_1}{n_0}$ and $f_2 \equiv \frac{n_2}{n_0}$ are the population ratios of the $^3P_1$ and $^3P_2$ levels respectively, relative to

the population of $^3P_0$. We are ignoring the populations of the more highly excited electronic states, which are negligible at these temperatures and densities. By using the principle of detailed balance and knowing the excitation cross-sections for $e^- - O^{++}$ collisions (Spitzer, 1978), the quantities $f_1$ and $f_2$ can be calculated as functions of electron density and temperature, as shown in Figure 1. Thus, Equation (1) has two uses: (a) with an assumed $O^{++}$ abundance and a value for $n_e$, one can predict the strengths of the 51.8μm and 88.35μm lines; or (b) with a measurement of the strength of either line one obtains directly a value for the $O^{++}$ column density. Inspection of Figure 1 shows that the population of the $^3P_1$ level as a fraction of the total population is relatively constant over a large range of electron densities, and hence observation of the 88.35μm transition alone gives an accurate measure of the $O^{++}$ column density, even when large uncertainties exist in the assumed electron density. Relative abundances of two ionic species which both have far-infrared fine structure lines can hence also be well determined by measurements of this type.

To derive a fractional abundance of $O^{++}$ relative to hydrogen, an accurate value for the electron column density is required. The derivation of electron column densities from radio continuum data is difficult, however, because it is necessary to model the source with a shape and structure in order to determine the relation between electron column density ($n_e l$) and emission measure ($n_e^2 l$). Only in very

simple cases can the electron density be determined accurately from the emission measure, and this represents a major source of uncertainty when fractional abundances are calculated on this basis.

An alternative approach is to measure the intensities of both the [O III] lines, allowing the electron density to be determined in a more direct manner. From detailed balance in the $^3P$ term, the following relation can be easily derived:

$$n_e = \frac{\gamma_{01}\left(A_{21} + A_{20}\right) + \gamma_{02}\left(A_{21} - \frac{R}{a} A_{10}\right)}{\gamma_{01}\left(\frac{R}{a}\gamma_{12} - \gamma_{21} - \gamma_{20}\right) + \gamma_{02}\left[\frac{R}{a}\left(\gamma_{12} + \gamma_{10}\right) - \gamma_{21}\right]} \qquad (2)$$

where $\gamma_{ij}$ is the collisional rate coefficient for the transition i→j (see Spitzer 1978), $A_{ij}$ is the A-coefficient for the transition i→j, $a \equiv (51.8/88.35)(A_{10}/A_{21}) = 0.158$, and $R \equiv I(88.35\mu m)/I(51.8\mu m)$ is the ratio of the observed line intensities. A procedure similar to this for determining $n_e$ has already been employed by Melnick, Gull, and Harwit (1979b), and produces values of $n_e$ significantly different from the radio-determined values. While this method is more direct, it suffers from two difficulties. First, the ratio of intensities, R, does not vary linearly with $n_e$ but for a given fractional change in density changes very slowly at both the high and low ends of the range of typical densities. Thus the derived value for $n_e$, which represents an average of the dependence upon $n_e$ of R over the line of sight, should be a lower limit to the average value of $n_e$ and may be considerably lower than the true value. It is thus anomalous that some of the values for $n_e$ derived via this method by Melnick et al.

are higher than the rms values of $n_e$ obtained from emission measures, which should be upper limits to the average value of $n_e$. Secondly, conversion of $n_e$ to a column density requires knowledge of the line of sight length of the emitting region, and hence the size of the object must be well known.

b) [O I] $\lambda$ = 63.2μm

The ground term of neutral oxygen has $^{2S+1}L_J = {}^3P_{2,1,0}$, just like $O^{++}$, but the fine structure triplet is inverted as shown in Figure 2. As before, the most important transitions are the M1 transitions, $^3P_0 \rightarrow {}^3P_1$ (145.4μm*) and $^3P_1 \rightarrow {}^3P_2$ (63.20μm). The collisional excitation processes for O I are very different from O III, though, for two important reasons. First, O I is neutral, so the cross-sections for electron collisions will not be as large and electron collisions will not be as predominant an excitation mechanism. Secondly, O I has an ionization potential of 13.618 eV compared to 13.598 for hydrogen, so much of the neutral oxygen will be outside of the H II region and depend upon collisions with hydrogen atoms for excitation. The fact that O I is a constituent of the H I - H II transition region makes these fine structure lines very important for studying the structure of ionization fronts. It also makes prediction of the strengths of these lines very difficult. It is beyond the scope of this paper to study this problem in detail; we can, however, make a few reasonable estimates.

*taken from the data presented in Bashkin and Stoner (1976), which is more accurate than the compilation of Moore (1949) that led to the previously-accepted value of 147μm.

Examination of the collisional rate coefficients for oxygen collisions with protons (Bahcall and Wolf, 1968), electrons (Saraph, 1973) and hydrogen atoms (Launay and Roueff, 1977) finds the electron rates to be smaller than, but competing with, the proton rates. The hydrogen rates are down a factor of about 10 from the other two for the same temperature and density. Since the hydrogen collisions will contribute only in the lower-temperature non-ionized region, it is possible that the emission from this source will be a factor of ∿100 down from the emission from the ionized side. Taking electrons and protons to dominate the excitation, we can produce the population ratios in the $^3P$ term shown in Figure 2. Prediction of the [O I] intensities then follows directly from an assumed oxygen column density.

## III. RESULTS

### a) [O III]

We were able to observe only the 88.35μm line in this flight series. Figure 3 shows the result of a pair of observations; each represents two 40-second scans of the indicated wavelength range, or a total of about 15 seconds of integration on the line itself. The profiles were fitted by a least-squares procedure with a lorentzian line shape, which is a good approximation to our instrumental response. We therefore report peak intensity rather than integrated flux, as it is assumed that the line is substantially narrower than our resolution. At 88.35μm our resolution was sufficient to

bring the [O III] line well clear of all atmospheric water vapor lines, and no correction needs to be made for absorption.

Because the fine structure line and the 88μm continuum are recorded simultaneously by the spectrometer, our maps have essentially perfect registration between these two components. One expects the peak of the fine structure emission to be coincident with the maximum radio continuum emission, and this appears to be the case in all the sources we observed. We can thus determine the position of the far-infrared continuum peak in these sources with some certainty, relating it to radio peak positions which are usually known to high accuracy.

Table 1 is a summary of our intensities for the brightest peak in each source, together with predicted intensities and derived $O^{++}$ column densities. In the latter two quantities we have used an electron temperature of 8000 K, with electron densities and sizes of H II regions from the 15 GHz, 2 arc-minute resolution work of Schraml and Mezger (1969)--except for G29.9-0.0, for which we referred to Zeilik (1977). The predicted intensities for the H II regions assume an $O^{++}$ abundance of $1.5 \times 10^{-4}$ relative to hydrogen. This is derived from a cosmic oxygen abundance of $6.6 \times 10^{-4}$, of which 23% is assumed to be in the form of $O^{++}$. The predictions for the observed planetary nebulae NGC 7027 and NGC 6572 are due to Simpson (1975).

In principle it is possible to use our $O^{++}$ column densities to derive values for the $O^{++}$ fractional abundance by comparing them to the electron column densities. However, electron densities are subject to a number of uncertainties, as discussed in Section IIa, so that reliable values of the $O^{++}$ fractional abundances cannot yet be derived. In Table 2 we show first the electron densities and linear sizes of the nebulae derived from radio data, and the $O^{++}$ fractional abundances derived from these estimates. In the next three columns are the electron densities from Melnick et al. (1979b), the nebular sizes from this present work, and the $O^{++}$ fractional abundances derived on this basis. In addition, the fractional abundances obtained by Melnick et al. are listed. It is clear that substantial differences result from the use of different techniques for estimating electron column densities. This problem is likely to remain until more detailed models of the nebulae can be produced. It is also apparent that our values for the $O^{++}$ abundance are considerably lower than those of Melnick et al., who used source dimensions based on radio data and hence underestimated the size of the emitting region. We thus do not find it necessary to argue for an increase in the commonly accepted oxygen abundance ratio.

Figures 4-6 are the contour maps we have obtained. In each map, the positions where data was taken are marked by crosses; the data at each point was usually in the form of a pair of 40-second scans. Solid contours show the [O III] $\lambda$ = 88.35μm line intensity in units of $10^{-17}$W cm$^{-2}$, and the dotted contours show the continuum intensity in our 0.19μm

effective bandwidth ($\pi/2$ times the resolution), in the same units.

In each case studied we find that the far-infrared continuum is not centered on the peak of the ionization. Although this is not an unexpected result, it suggests that simple spherical models of H II regions which have the dust uniformly mixed with the ionized material will not give realistic predictions of the detailed properties of these sources.

In most sources examined the fine structure line intensity is distributed rather widely and smoothly. This is in part because our beam width of 1 arcminute is larger than some of the fine spatial structure, but in part must represent the actual widespread and relatively smooth distribution of [O III] in regions where the density is rather low and the Strömgren spheres of the ionizing stars are very large and tend to overlap.

We report below the details of the results from individual objects.

i) M17

In this source we mapped the far-infrared continuum simultaneously with the 88.35μm line, as shown in Figure 4. The peak [O III] emission is centered at the peak of the radio continuum (G15.0-0.7) and closely follows the radio contours, extending for several arcminutes along a northwest-southeast line. We also looked for and detected [O III] at one position

in the bright optical region to the northeast, at an intensity of $1.9 \times 10^{-16}$ W cm$^{-2}$. This position is close to the peak B observed by Montgomery et al. (1971) at 3.4 mm. No emission ($<2 \times 10^{-17}$ W cm$^{-2}$, $3\sigma$) was seen from the 90μm northern source of Lada (1976). The peak [O III] intensity is in reasonable agreement with the value predicted from the radio data. The total [O III] intensity is also consistent with that measured by Dain et al. (1978) in a 4' x 4.4' beam.

It is clear that the [O III] emission is very widespread, and probably extends well beyond the limits of our map. This supports the contention of Lada (1976) that a large group of stars have formed along the edge of the molecular cloud and are supplying an enormous flux of ionizing photons.

The 88μm continuum radiation forms an extended ridge along the molecular cloud to the southwest of the [O III] peak. This is similar to the recent findings of Wilson et al. (1979) who suggest that thermal emission from dust at the interface of the ionized region and the molecular cloud is responsible. We find that the continuum emission peaks at the northern edge of the ridge. Wilson et al. do not see such a peak at 69μm, and it is possible, although unlikely, that the discrepancy is due to the different wavelength used. An earlier map by Harper et al. (1976) has been made at 100μm, but at their resolution of 2.3 arcminutes the continuum peak appeared coincident with the radio source G15.0-0.7.

ii) NGC 7538

This is the first detection of the [O III] line in this source. The observed peak intensity is in good agreement with the value predicted from radio studies, assuming an $O^{++}$ fractional abundance of $1.5 \times 10^{-4}$. 21 cm interferometry by Israel et al. (1973) shows that the ionization resembles a section of a spherical shell centered on a point to the northeast of the peak emission. The [O III] peaks in the same place as the radio continuum and shows a similar structure (see Figure 5) though we do not resolve the bright condensations. We observe maximum far-infrared continuum at the position of IRS2 (Wynn-Williams et al. 1974), in agreement with recent work by Werner et al. (1979). At this position no [O III] is observed ($<2 \times 10^{-17}$W cm$^{-2}$, 3$\sigma$), consistent with the upper limit of $4 \times 10^{-17}$W cm$^{-2}$ of Moorwood et al. (1978).

iii) W51

The results of observations in this source are shown in Figure 6. As expected, the maximum [O III] emission comes from the region of most intense 5 GHz radio continuum, designated G49.5e by Martin (1972). This position is coincident with the infrared source IRS1 (Wynn-Williams et al. 1974). The far-infrared continuum peaks somewhat to the north and west of this source, close to the maximum 55μm continuum observed by Harvey et al. (1975). In contrast with the 55μm result, however, we find the far-infrared continuum to be

quite extended, implying a widespread distribution of cooler dust throughout the ionized material. Although we cannot rule out the possibility that the far-infrared peak is centered on IRS2, it does appear more likely that it lies between IRS1 and IRS2.

Using the electron density and linear size that Martin derives for G49.5e, we can predict a value of $0.9 \times 10^{-16}$W cm$^{-2}$ in the [O III] line for this peak, in better agreement with the observations than the prediction in Table 1, based on the lower resolution 15 GHz data.

iv) W49A

Although we were able to detect [O III] in this source, no attempt was made to map the spatial distribution. Refering to Table 1, it is clear that our observed value for the peak flux is considerably lower than that predicted from the radio work of Schraml and Mezger. This may be because much of the flux seen by Schraml and Mezger is due to bright condensations (Wynn-Williams, 1971) too small for us to resolve. This would imply that $\langle n_e^2 \rangle \geq 60(\langle n_e \rangle)^2$, i.e. rather extreme conditions with ionization condensations filling perhaps 10% of the beam. Another possibility is that the underlying stars are too cool to ionize much of the oxygen to $O^{++}$, and hence that the fractional abundance of this ion is low. It would be interesting to search for the 10.52μm line of [S IV] (required ionizing energy 34.8 eV; essentially the same as for O III) to test this possibility.

v) W3

W3A is unresolved by our beam; the peak [O III] emission seems to be in the direction of W3-IRS1 (Wynn-Williams et al. 1972). Negligible [O III] was observed in positions 1' north, 1' south, 1' east and 1' west of the peak, or from IRS4.

Our observations of IRS3 show no emission, but the upper limit is only about half that of the detection in IRS1. Unfortunately IRS3 was only observed at the beginning of the flight series, when the spectrometer was adjusted for low resolution and hence unable to discriminate well against the continuum of the source. The total intensity we see ($1.0 \times 10^{-16}$W cm$^{-2}$) is considerably lower than that seen by Dain et al. (1978) ($3.1 \times 10^{-16}$W cm$^{-2}$), but higher than the upper limit of Moorwood et al. (1978) ($<7 \times 10^{-17}$W cm$^{-2}$). Although W3A appears to be a point source, it is possible that the large beam used by Dain et al. included emission from regions we did not examine. This seems unlikely as all such regions have lower radio continuum flux than IRS1.

vi) M42 (Orion)

A number of positions in this source were observed, as shown in Figure 7. The emission peaks in the vicinity of the Trapezium, with an intensity of $1.2 \times 10^{-10}$W cm$^{-2}$sr$^{-1}$, in good agreement with the value of $1.1 \times 10^{-10}$W cm$^{-2}$sr$^{-1}$ observed by Moorwood et al. (1978). These authors found that the decrease in emission intensity with increasing distance from the Trapezium was very gradual. The present data,

taken at a different series of positions, present further evidence for a very uniform distribution of [O III] emission. We see an intensity of 70% of the peak value at each of the four points 2 arcminutes away from the Trapezium, and a continued gradual fall-off at the positions to the northeast and southwest.

Altogether the distribution of emission is considerably more uniform than that predicted by the model of Simpson (1973). There is also a significant difference between our data points 2 arc minutes north and east and 2 arc minutes south and west, showing that even at 1 arcminute resolution the assumption of spherical symmetry for the source is not very realistic.

Under the assumption of a homogeneous cloud with uniform ionization fraction throughout, the [O III] line intensity should be approximately proportional to the square root of the radio continuum flux. Comparison with the 15 GHz data of Schraml and Mezger (1969) does show some such correlation, but also significant differences. Variations in the density of the ionized gas are most likely responsible for these differences. Qualitatively they correspond to the presence of low density ($n_e \gtrsim 100$ cm$^{-3}$) material along the line of sight, presumably in front of the denser ionized region which produces most of the radio continuum. Since M42 is so large and time on the source was limited, a complete map on the scale of our beam size was not attempted. It is clear that

a detailed study of the Orion nebula in the [O III] line would provide a valuable probe of low density ionized material and of ionization conditions, particularly in the obscured regions such as the dark bay to the east.

b) [O I]

Observations of the [O I] line were hampered by a lower system performance at this wavelength. The flight schedule did not allow observation of Jupiter at 63μm, and hence for calibration we must rely on observations of the moon and of the far-infrared continuum of the sources themselves. In addition, there is a strong atmospheric water vapor line at 63.3μm. Although this line is quite narrow and does not attenuate the [O I] emission, it absorbs an unknown amount of the continuum radiation adjacent to the [O I] line and hence produces an apparent decrease in the line intensity. This effect is most important for the stronger continuum sources. The atmospheric water vapor content can change by a factor of 3 or more during a flight, and is a strong function of altitude. Because of these uncertainties our estimates of the absolute [O I] intensities are limited to an accuracy of about 50%.

Ionospheric [O I] emission at 63.2μm has recently been detected by Grossman and Offermann (1978). Although the intensities they see are comparable to our observed values, our use of beam switching throughout the flights eliminates any possibility of contamination from this source. In principle an optically deep ionospheric line could severely

attenuate the astronomical line; however calculation shows this not to be a problem.

In Table 3 we present the observed [O I] intensities, together with predicted intensities based on the radio data of Schraml and Mezger (1969) and an assumed fractional oxygen abundance of $1.5 \times 10^{-4}$. The predicted [O I] intensities are in qualitative agreement with our results, although too much reliance should not be placed on the predictions. The excitation of neutral oxygen in H I - H II transition regions is a complex problem that deserves a great deal more theoretical attention, as well as additional observations. A detailed discussion of [O I] emission from weak D-type ionization fronts and shocked molecular clouds is available in a recent paper by Hill and Hollenbach (1978).

i) M17

We have detected the line in the direction of the peak radio emission in M17, with an intensity of $1.2 \times 10^{-16}$W cm$^{-2}$. Although no attempt was made to map this source, comparison with the result of Melnick et al. (1979a) of $24 \times 10^{-16}$W cm$^{-2}$ in a 4 x 6 arcminute beam (an area 15 times larger than ours) suggests that the emission is widely spread throughout the nebula.

ii) DR21

This is the first detection of a far-infrared fine structure line in this source. The observed flux is $8.1 \times 10^{-17}$W cm$^{-2}$, and although random noise is low, the

difficulties of correction properly for the atmospheric vapor prevent us from ascribing more than a 3σ certainty to this detection.

### iii) M42 (Orion)

Several points throughout the nebula were observed, as shown in Figure 8. It is apparent that the majority of the [O I] emission is from the ionized regions, or more probably from the ionization fronts associated with the H II regions. This is shown in the strong emission coming from the bright optical bar to the southeast, which also shows up strongly in the 6300 Å line of [O I] (T. R. Gull, 1978). The strongest signal we see is at the Trapezium, $1.3 \times 10^{-16}$ W cm$^{-2}$. Assuming that the emitting region uniformly fills the effective 75 arcsecond disc of our beam, this corresponds to a flux at the surface of the nebula of 0.039 erg sec$^{-1}$cm$^{-2}$. This is comparable to the values predicted by Hill and Hollenbach (1978) for the total ionization front plus shock front emission following a 5-10 km s$^{-1}$ shock. However, since no molecular hydrogen radiation is seen from regions strong in [O I] emission nor is much [O I] emission seen from around KL where the vibrationally excited $H_2$ emission is most intense, it seems clear that shocks are not the main mechanism for exciting [O I]. The expected alternative location for forming the [O I] line is in the transition zone between H II regions and the neutral material; these are in fact the regions we observe to be most intense.

If the Trapezium is indeed the brightest source of [O I] emission, then our observed surface brightness is in conflict with the value of 0.13 erg $sec^{-1}cm^{-2}$, averaged over the whole nebula, determined by Melnick et al. (1979a). Two possible explanations are (a) the majority of the emission comes from regions we did not observe, or (b) our chopper throw of 5 arcminutes was insufficient to bring our reference beam clear of the emission. Neither explanation appears attractive, however, and it is more likely that the difference is due to the great difficulty of correcting properly for atmospheric absorption so close to a water vapor line. Observations at higher spectral resolution than has so far been used would resolve this difficulty in a straightforward manner. Even allowing a factor of two error in each of the two measurements, a very widespread distribution of [O I] is implied by the large amount of flux in the 6 x 4 arcminute beam relative to the 75 arcsecond beam. This is further evidence against a shock mechanism being the primary source of excitation of the line.

c) HD

The HD molecule has a dipole moment of $5.9 \times 10^{-4}$D (Trefler and Gush, 1968), resulting in a pure rotational spectrum, the J=1→0 transition of which falls at 112.08μm. The Einstein A-coefficient of this transition is $2.54 \times 10^{-8}$ $sec^{-1}$, and the transition is thus in thermal equilibrium at quite low densities. Calculation of expected line intensities is similar to the case of atomic fine structure lines,

but with molecular hydrogen as the principal collision partner. For example, Bussoletti and Stasinska (1975) have predicted the flux from the Orion molecular cloud as $1.1 \times 10^{-16}$ W cm$^{-2}$ for the 112μm line.

We searched for this transition in the direction of the Kleinmann-Low nebula, but after five minutes of integration the baseline stability became the limiting factor, due to a combination of the lower resolution used at this wavelength ($\lambda/\delta\lambda \approx 180$) and the high continuum level of the source. The upper limit we obtain of $6 \times 10^{-17}$ W cm$^{-2}$ in our beam is not sufficiently low to rule out any but very optimistic models of the Orion molecular cloud. On the other hand, increased spectral resolution and other feasible improvements to the spectrometer should allow detection of this and other far-infrared molecular lines in warm clouds.

## ACKNOWLEDGMENTS

We wish to thank the staff of the Kuiper Airborne Observatory for their dedication and enthusiasm. T. Mathieson and A. Meyer were also particularly helpful. M. Harwit, J.-P. Baluteau and T. Gull made data available to us prior to publication. W. Fitelson duplicated the entire spectrometer electronics in a few weeks to provide us with spare circuit cards. K. Shivanandan supplied us with the detector and integrating cavity, which contributed significantly to the improved performance of our new spectrometer.

## REFERENCES

Bahcall, J.N. and Wolf, R.A. 1968, Ap. J., 152, 701

Baluteau, J.-P., Bussoletti, E., Anderegg, M., Moorwood, A.F.M. and Coron, N. 1976, Ap. J. Lett., 210, L45

Bashkin, S. and Stoner, J.O. 1975, Atomic Energy Levels and Grotrian Diagrams (North-Holland, Amsterdam)

Bussoletti, E. and Stasinska, G. 1975, Astron. Astrophys., 39, 177

Dain, F.W., Gull, G.E., Melnick, G., Harwit, M. and Ward, D.B. 1978, Ap. J. Lett., 221, L17

Grossmann, K.U. and Offermann, D. 1978, Nature, 276, 594

Gull, T.R. 1978, private communication

Harper, D.A., Low, F.J., Rieke, G.H. and Thronson, H.A. (Jr.) 1976, Ap. J., 205, 136

Harvey, P.M., Hoffman, W.F. and Campbell, M.F. 1975, Ap. J. Lett., 196, L31

Hill, J.K. and Hollenbach, D.J. 1978, Ap. J. 225, 390

Israel, F.P., Habing, H.J. and deJong, T. 1973, Astron. Astrophys., 27, 143

Lada, C.J. 1976, Ap. J. Suppl. Ser., 33-C1, 603

Launay, J.M. and Roueff, E. 1977, Astron. Astrophys., 56, 289

Martin, A.H.M. 1972, Mon. Not. R. Astron. Soc., 157, 31

Melnick, G., Gull, G.E. and Harwit, M. 1979a, Ap. J. Lett., 227, L29

Melnick, G., Gull, G.E. and Harwit, M. 1979b, Ap. J. Lett., 227, L35

Montgomery, J.W., Epstein, E.E., Oliver, J.P., Dworetsky, M.M. and Fogarty, W.G. 1971, Ap. J., 167, 77

Moore, C.E. 1949, Atomic Energy Levels, NSRDS-NBS35, National Bureau of Standards, Washington D. C.

Moorwood, A.F.M., Baluteau J.-P., Anderegg, M., Coron, N. and Biraud, Y. 1978, Ap. J., 224, 101.

Saraph, H.E. 1973, J. Phys. B., 6, L243

Schraml, J. and Mezger, P.G. 1969, Ap. J., 156, 269

Simpson, J.P. 1973, Publ. Astron. Soc. Pac., 85, 479

Simpson, J.P. 1975, Astron. Astrophys., 39, 43

Smith, H.A. 1969, Ap. J. 158, 371

Spitzer, L. 1978, Physical Processes in the Interstellar Medium (Wiley-Interscience, New York)

Trefler, M. and Gush, H.P. 1968, Phys. Rev. Lett., 20, 703

Ward, D.B., Dennison, B., Gull, G. and Harwit, M. 1975, Ap. J. Lett., 202 , L31

Werner, M.W., Becklin, E.E., Gatley, I., Matthews, K., Neugebauer, G. and Wynn-Williams, C.G. 1979, to be published

Wilson, T.L., Fazio, G.G., Jaffe, D., Kleinmann, D., Wright, E.L. and Low, F.J. 1979, to be published.

Wynn-Williams, C.G. 1971, Mon. Not. R. Astron. Soc., 151, 397

Wynn-Williams, C.G., Becklin, E.E. and Neugebauer, G. 1972, Mon. Not. R. Astron. Soc. 160, 1

Wynn-Williams, C.G., Becklin, E.E. and Neugebauer, G. 1974, Ap. J., 187, 473

Zeilik, M. (II) 1977, Ap. J., 218, 118

Table 1

Summary of [O III] Results

| Source | $\alpha(1950)^{\dagger}$ | $\delta(1950)^{\dagger}$ | Observed [O III] Intensity ($10^{-16}$ W cm$^{-2}$) | Predicted [O III] Intensity ($10^{-16}$ W cm$^{-2}$) | Derived $O^{++}$ Column Density ($10^{17}$ cm$^{-2}$) |
|---|---|---|---|---|---|
| M17 | $18^h17^m34.^s5$ | -16°13'24" | 3.9 | 2.8 | 16.8 |
| NGC 7538 | $23^h11^m22.^s9$ | +61°13'50" | 1.3 | 0.98 | 6.8 |
| M42 | $5^h32^m49.^s6$ | -5°25'16" | 1.2 | 1.6 | 5.1 |
| W51 | $19^h21^m23.^s0$ | +14°24'54" | 1.1 | 4.4 | 4.2 |
| W3A | $2^h21^m55.^s0$ | +61°52'00" | 1.0 | 1.6 | 4.2 |
| W49A | $19^h7^m55.^s9$ | +9°01'01" | 0.56 | 4.3 | 2.9 |
| M82 | $9^h51^m44.^s0$ | +69°55'04" | <0.26* | -- | -- |
| NGC 7027 | $21^h5^m9.^s4$ | +42°02'03" | <0.20* | 0.21 | -- |
| DR21 | $20^h37^m13.^s5$ | +42°03'51" | <0.20* | 0.15 | -- |
| NGC 6572 | $18^h9^m40.^s6$ | +6°50'25" | <0.16* | 0.10 | -- |
| G29.9-0.0 | $18^h43^m27.^s7$ | -2°42'48" | <0.12* | 0.09 | -- |

*3σ upper limit

†nominal positions only

Table 2

Derived $O^{++}$ Fractional Abundances

| | Radio | | | Far-Infrared | | | Melnick et al. |
|---|---|---|---|---|---|---|---|
| Source | $n_e$* ($cm^{-3}$) | $\ell$* (pc) | $O^{++}$ Fractional Abundance ($10^{-4}$) | $n_e$† ($cm^{-3}$) | $\ell$ (pc) | $O^{++}$ Fractional Abundance ($10^{-4}$) | $O^{++}$ Fractional† Abundance ($10^{-4}$) |
| M17 | 950 | 2.68 | 2.1 | 1450 | 3.5 | 1.0 | 3.8 |
| M42 | 2237 | 0.65 | 1.1 | 7080 | 0.67 | 0.40 | 5.0 |
| W51 | 957 | 4.29 | 0.37 | 1515 | 6.6 | 0.15 | 1.9 |
| NGC 7538 | 437 | 2.50 | 2.0 | -- | -- | -- | -- |
| W49A | 536 | 8.41 | 0.2 | -- | -- | -- | -- |

*taken from Schraml and Mezger (1969)

†taken from Melnick et al. (1979b)

Table 3

Summary of [O I] Results

| Source | α(1950) | δ(1950) | Observed [O I] Intensity ($10^{-16}$ W cm$^{-2}$) | Predicted [O I] Intensity ($10^{-16}$ W cm$^{-2}$) |
|---|---|---|---|---|
| M17 | $18^h17^m34^s.5$ | -16°13'24" | 1.2 | 2.0 |
| M42 | $5^h32^m49^s.6$ | -5°25'16" | 1.3 | 1.9 |
| DR21 | $20^h37^m13^s.5$ | +42°03'51" | 0.81 | 0.60 |

## FIGURE CAPTIONS

Fig. 1. Relative populations of the levels of the ground term of $O^{++}$ plotted as a function of electron density for four different electron temperatures. The inset shows the energy level diagram for the ground term of this ion. Comparison of this result with that of Smith (1969) shows that the effect of the higher-energy electronic states is negligible in this density range.

Fig. 2. Relative populations of the levels of the ground term of atomic oxygen plotted as a function of electron density for three different electron temperatures. The inset shows the energy level diagram.

Fig. 3. [O III] emission in M17 and NGC 7538. Each profile represents one pair of 40 second scans. A lorentzian profile has been fitted to the data via a least-squares procedure, yielding values for both the peak line intensity and the continuum level.

Fig. 4. Map of [O III] emission in M17 (solid contours) and 88μm continuum (dotted contours). The Δ marks a position on the bright optical bar where [O III] was detected at an intensity of $1.9 \times 10^{-16}$ W cm$^{-2}$.

Fig. 5. Map of [O III] emission in NGC 7538. The Δ marks the position of IRS2 (Wynn-Williams et al. 1974).

Fig. 6. Map of [O III] emission in W51 (solid contours) and 88μm continuum (dotted contours). The positions of IRS1 and IRS2 are from Wynn-Williams et al. (1974)

Fig. 7. The Orion nebula, showing positions at which [O III] data was taken with measured intensities in units of $10^{-17}$W cm$^{-2}$.

Fig. 8. The Orion nebula, showing [O I] data with intensities in units of $10^{-17}$W cm$^{-2}$.

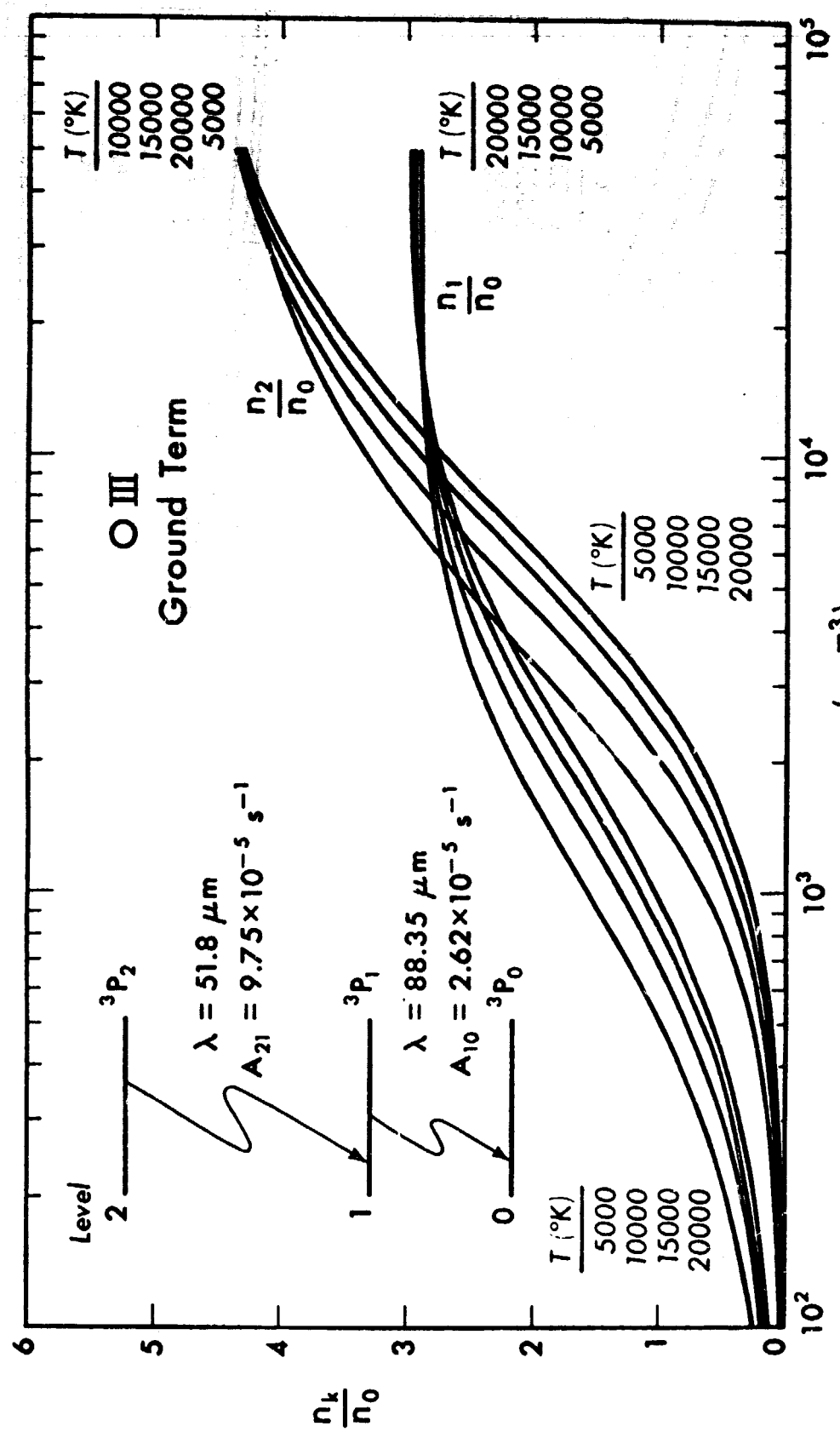
O III
Ground Term
Level
2
1
0
$^3P_2$
$^3P_1$
$^3P_0$
λ = 51.8 μm
$A_{21} = 9.75\times10^{-5}$ s$^{-1}$
λ = 88.35 μm
$A_{10} = 2.62\times10^{-5}$ s$^{-1}$
$\frac{n_2}{n_0}$
$\frac{n_1}{n_0}$
$\frac{n_k}{n_0}$
T (°K)
5000
10000
15000
20000
$n_e$ (cm$^{-3}$)
$10^2$
$10^3$
$10^4$
$10^5$
0
1
2
3
4
5
6

Fig. 1

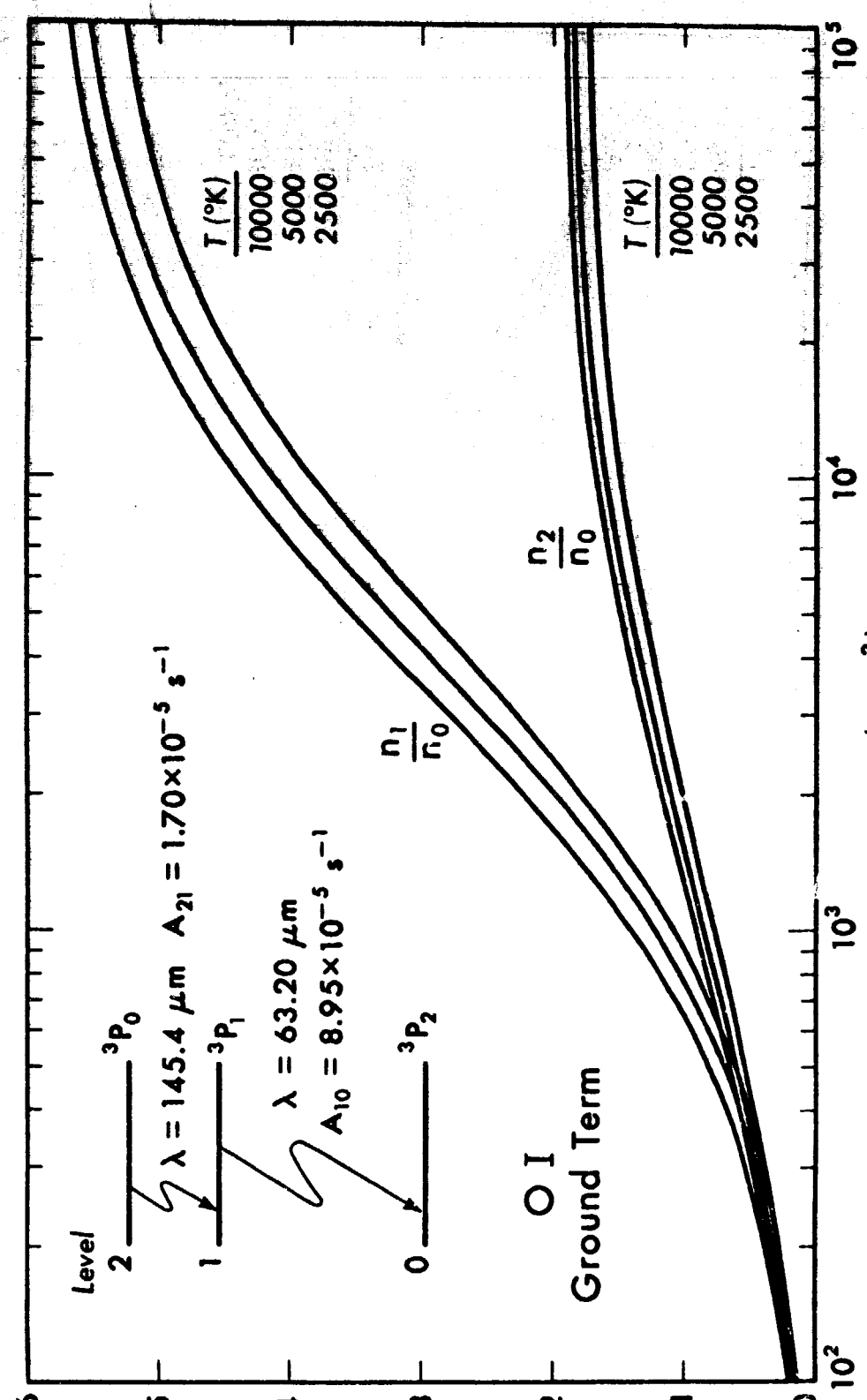


Fig. 2

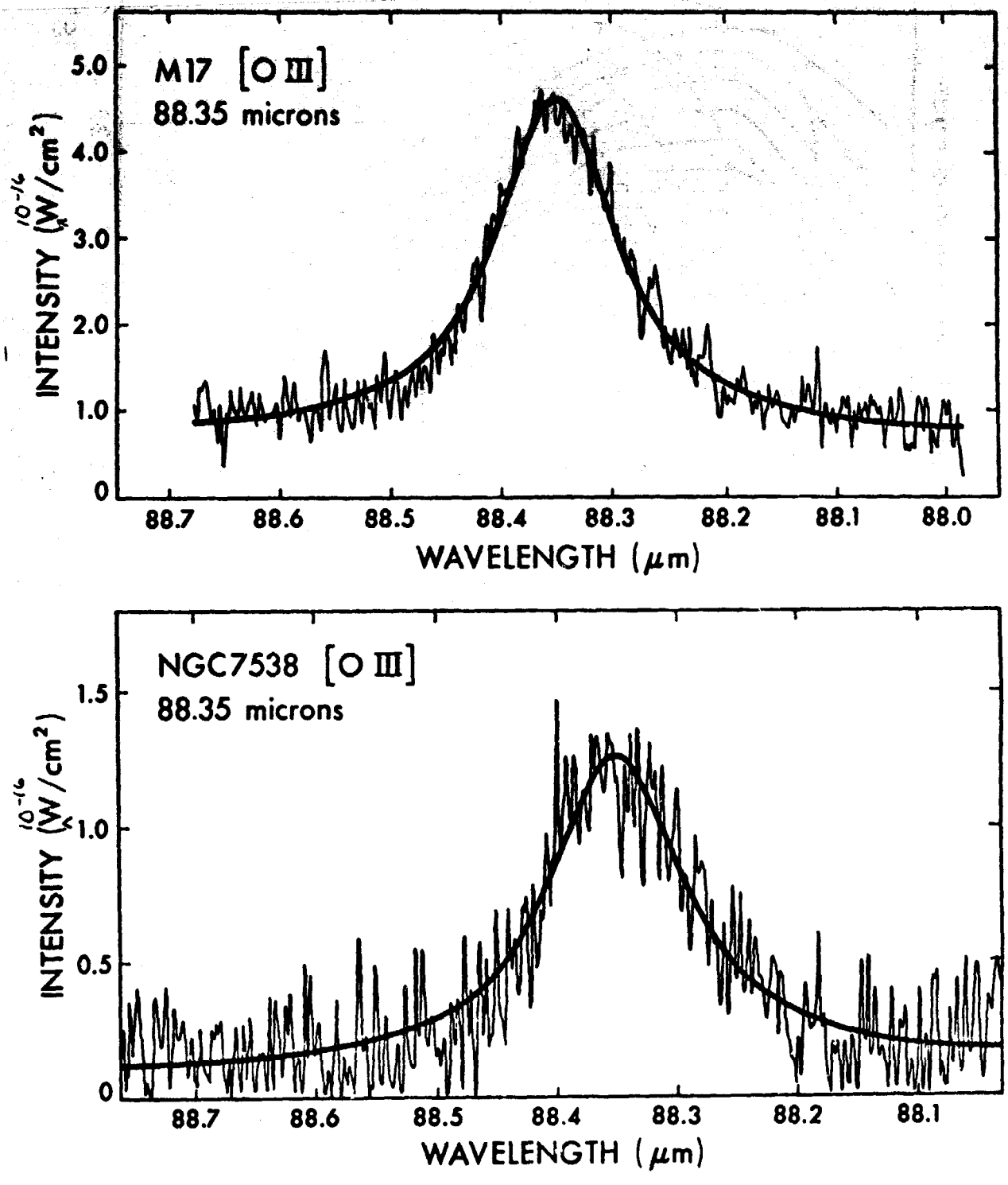


Fig. 3

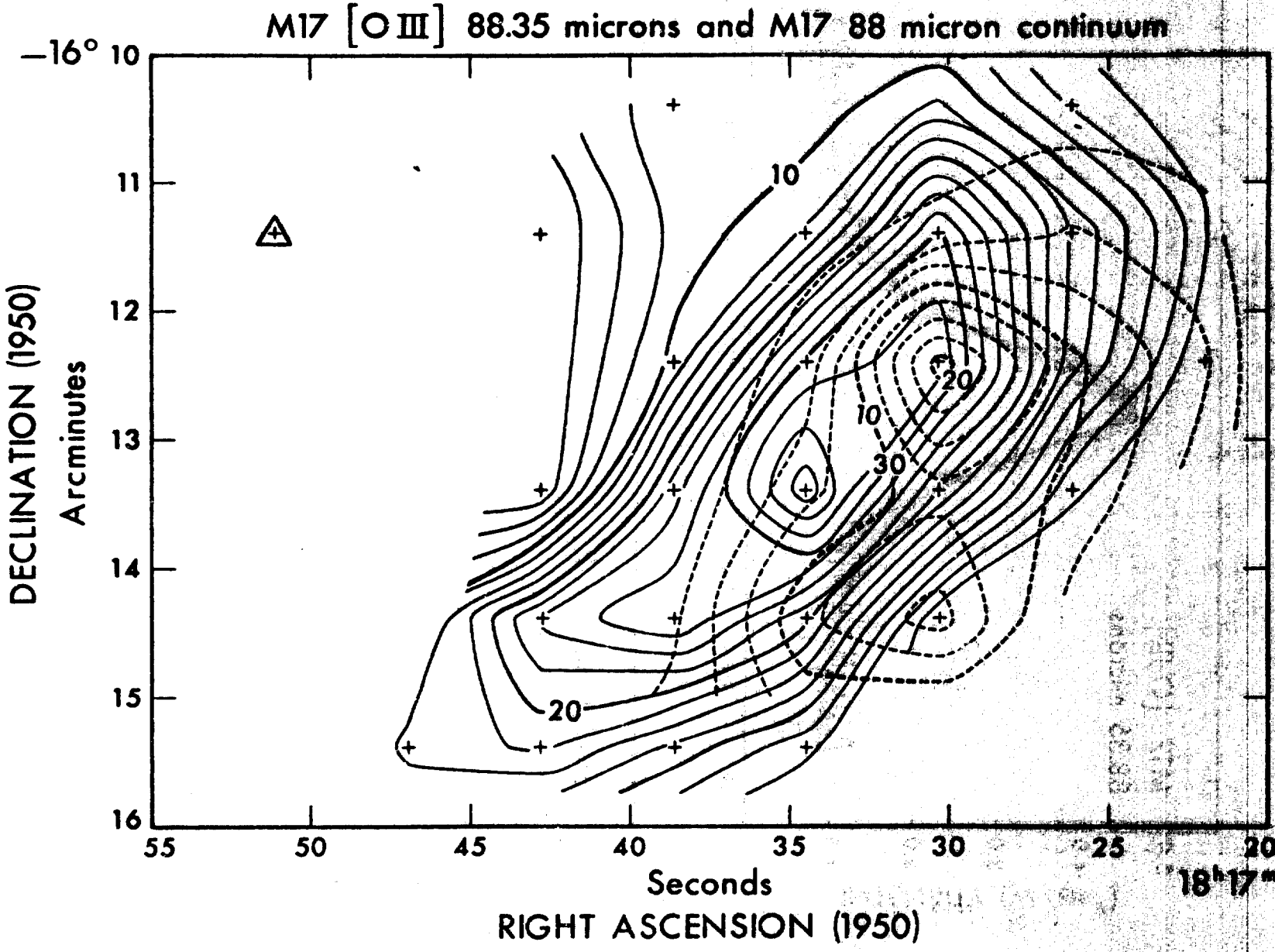
M17 [O III] 88.35 microns and M17 88 micron continuum
−16° 10
11
12
13
14
15
16
DECLINATION (1950)
Arcminutes
10
20
10
30
20
55
50
45
40
35
30
25
20
Seconds
18h17m
RIGHT ASCENSION (1950)

Fig. 4

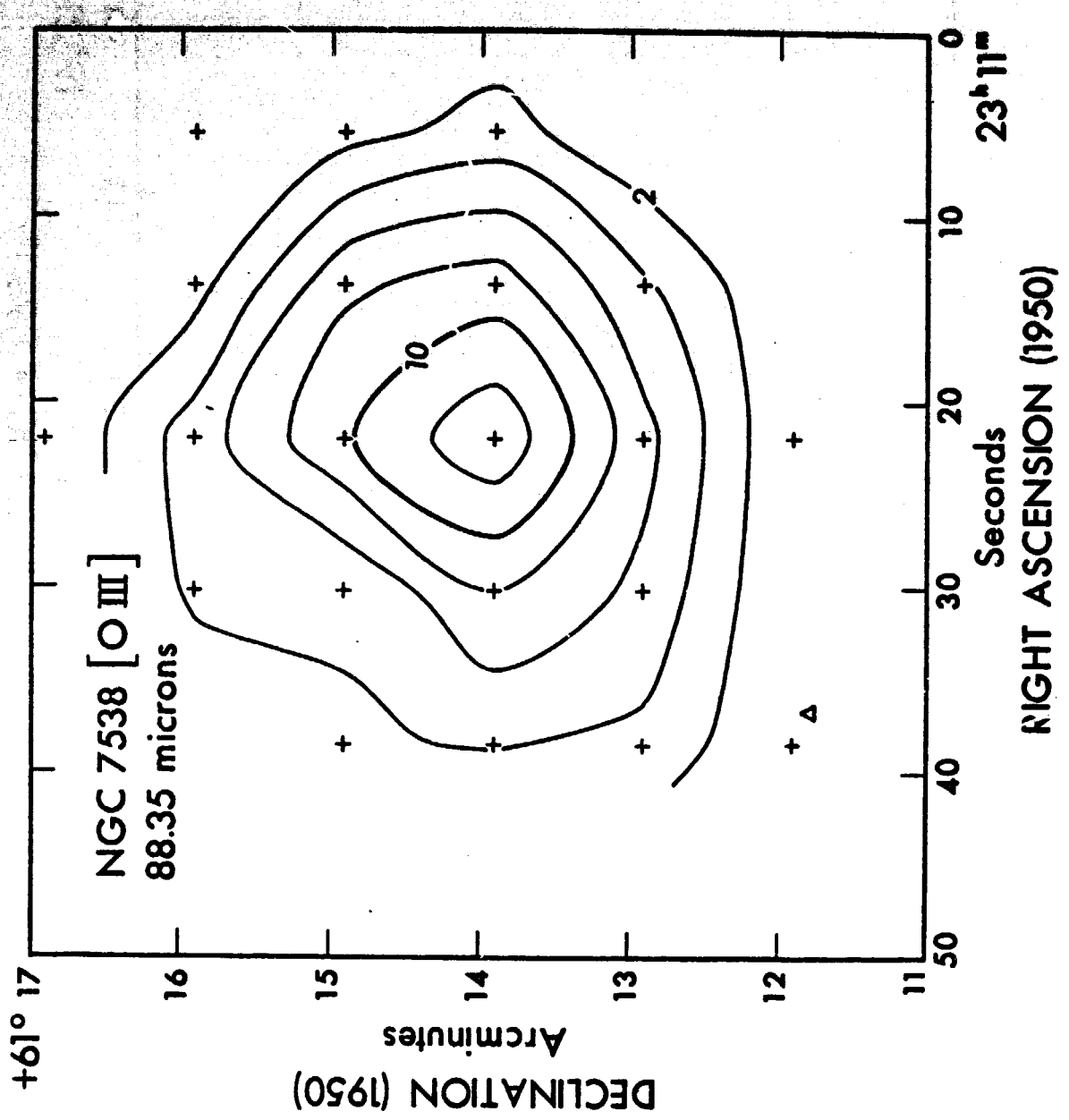
NGC 7538 [O III]
88.35 microns
2
10
+61° 17
16
15
14
13
12
11
Arcminutes
DECLINATION (1950)
50
40
30
20
10
0
Seconds
23h11m
RIGHT ASCENSION (1950)

Fig. 5

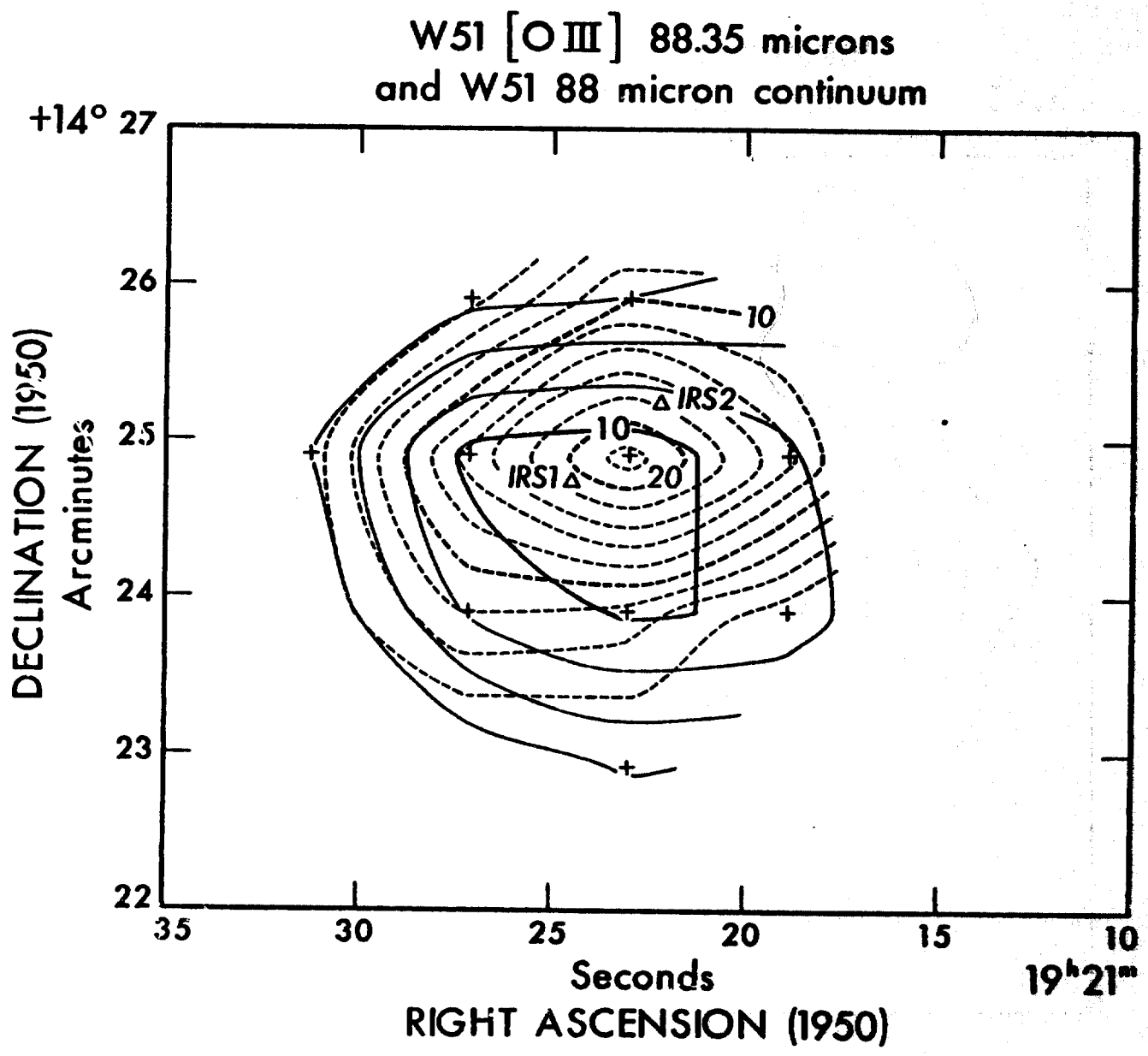
W51 [O III] 88.35 microns
and W51 88 micron continuum
+14° 27
26
25
24
23
22
DECLINATION (1950)
Arcminutes
10
IRS2
10
IRS1
20
35
30
25
20
15
10
Seconds
19h21m
RIGHT ASCENSION (1950)

Fig. 6

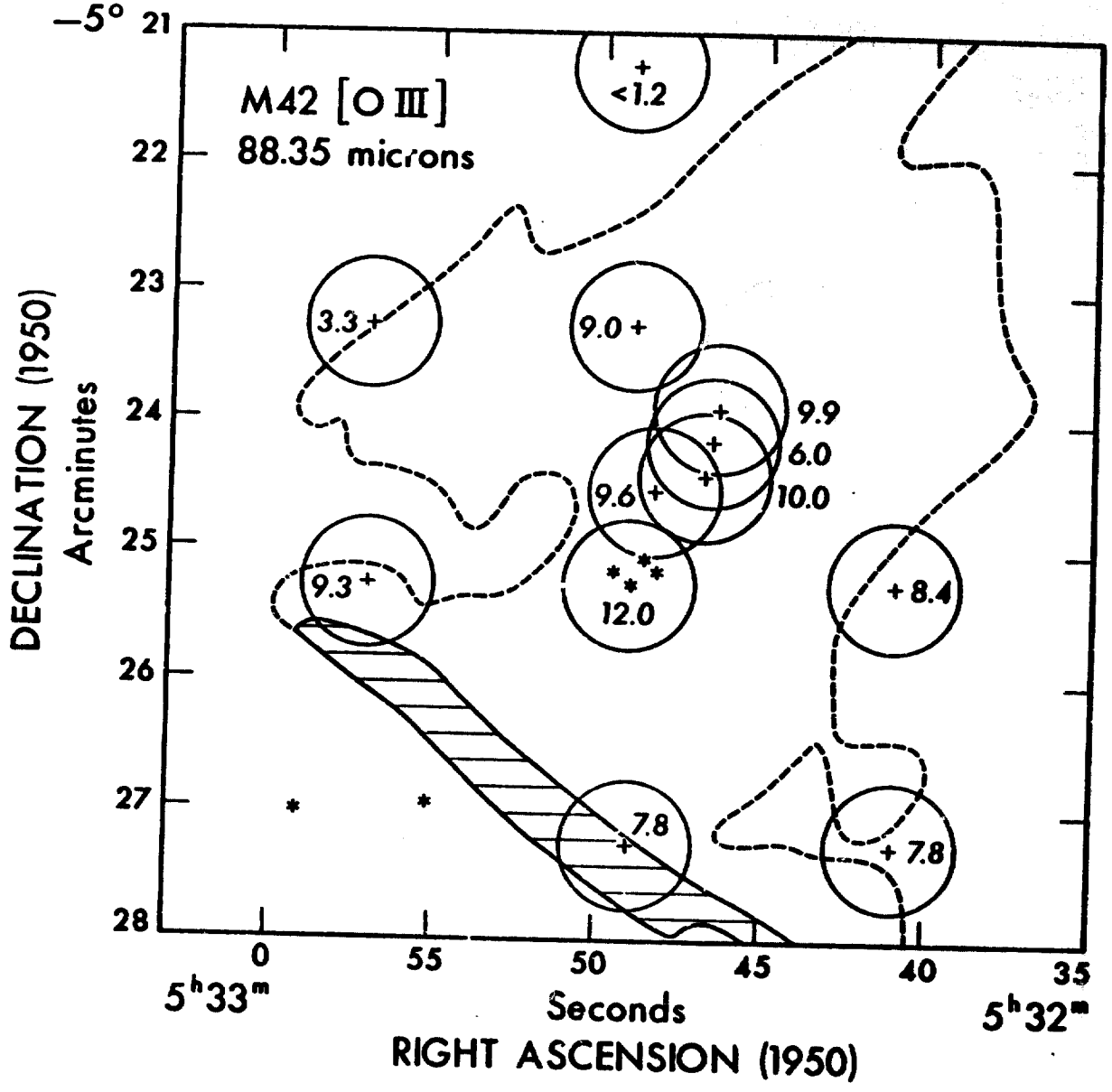
M42 [O III]
88.35 microns
<1.2
3.3
9.0
9.9
6.0
10.0
9.6
9.3
12.0
8.4
7.8
7.8
−5° 21
22
23
24
25
26
27
28
DECLINATION (1950)
Arcminutes
0
55
50
45
40
35
5h33m
Seconds
5h32m
RIGHT ASCENSION (1950)

Fig. 7

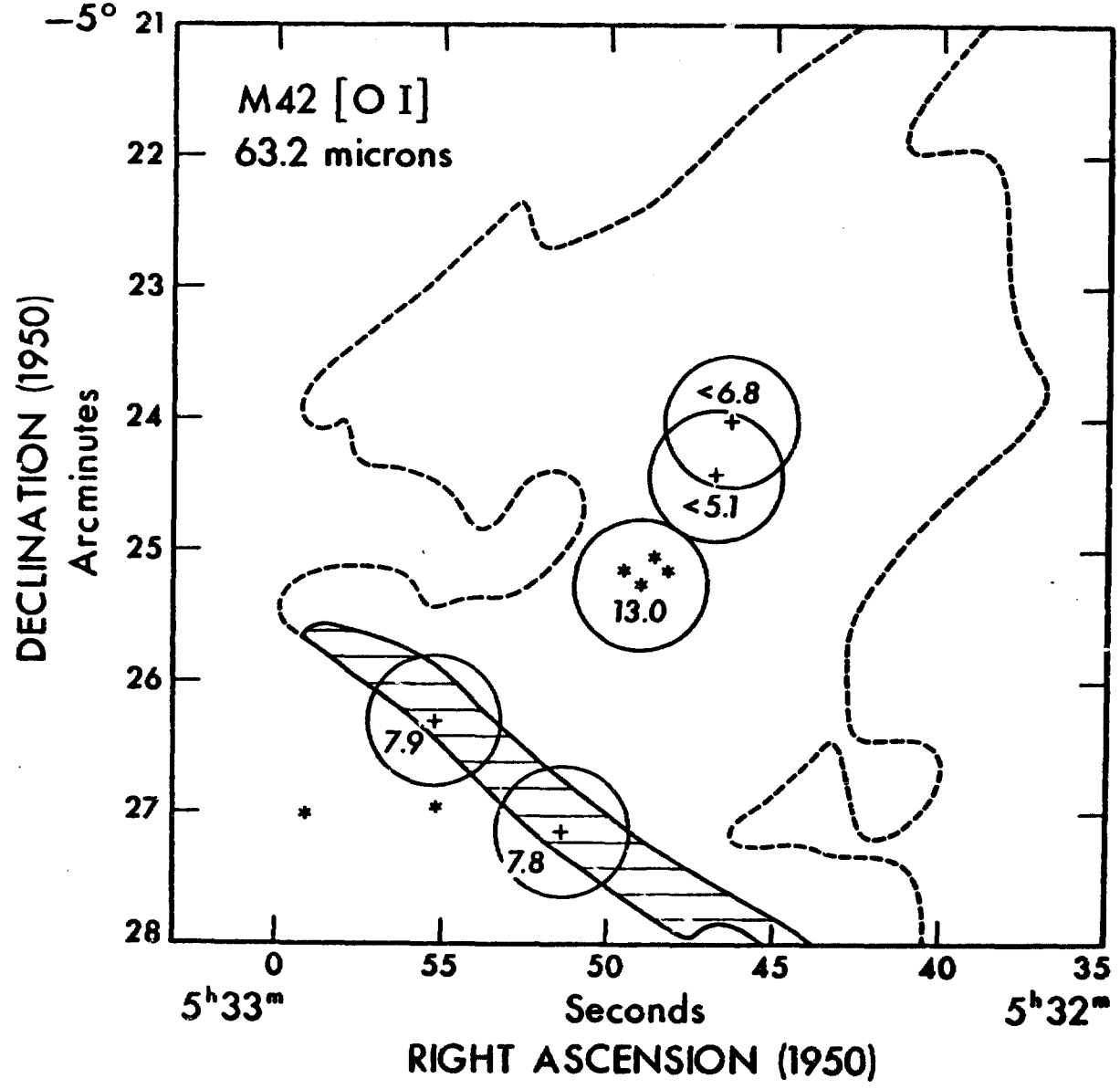
M42 [O I]
63.2 microns
<6.8
<5.1
13.0
7.9
7.8
−5° 21
22
23
24
25
26
27
28
DECLINATION (1950)
Arcminutes
0
55
50
45
40
35
5h33m
Seconds
5h32m
RIGHT ASCENSION (1950)

Fig. 8